# Crystallization Kinetics and Crystallization Behavior of Syndiotactic Polystyrene/Clay Nanocomposites

CHEN-RUI TSENG,[1] HSIN-YI LEE,[2] FENG-CHIH CHANG[1]

[1]Institute of Applied Chemistry, National Chiao-Tung University, Hsin-Chu, Taiwan, 30043

[2]Synchrotron Radiation Research Center, Hsin-Chu, Taiwan

*Received 7 November 2000; revised 8 June 2001; accepted 11 June 2001*

**ABSTRACT:** We investigated the effects of montmorillonite (clay) on the crystallization kinetics of syndiotactic polystyrene (sPS) with isothermal differential scanning calorimetry analyses. The clay was dispersed into the sPS matrix via melt blending on a scale of 1–2 nm or up to about 100 nm, depending on the surfactant treatment. For a crystallization temperature of 240 °C, the isothermal crystallization data were fitted well with the Avrami crystallization equation. Crystallization data on the kinetic parameters (i.e., the crystallization rate constant, Avrami exponent, clay content, and clay/surfactant cation-exchange ratio) were also investigated. Experimental results indicated that the crystallization rate constant of the sPS nanocomposite increased with increasing clay content. The clay played a vital role in facilitating the formation on the thermodynamically more favorable all-$\beta$-form crystal when the sPS was melt-crystallized. © 2001 John Wiley & Sons, Inc. J Polym Sci Part B: Polym Phys 39: 2097–2107, 2001
**Keywords:** montmorillonite; syndiotactic polystyrene; nanocomposites; crystallization kinetics

## INTRODUCTION

The synthesis of stereoregular polystyrene has been developed to produce nearly 100% syndiotactic conformation with a specific metallocene catalyst.[1–3] Syndiotactic polystyrene (sPS) differs from other polystyrenes (such as atactic polystyrene and isotactic polystyrene) in that phenyl rings regularly alternate from side to side with respect to the polymer chain backbone. This highly stereoregular sPS has attracted increasing attention because of its commercial importance. sPS can be crystallized into two different chain conformations, helical and trans. Helical (TTGG) conformations are formed in solution-recovered sPS, whereas the more favorable all-trans (TTTT) conformations are formed either from the melt or from annealing at elevated temperatures.[4–8] Blends of thermoplastic polymers with montmorillonite have been extensively studied because small amounts of well-dispersed clay in polymer matrices can improve their mechanical properties, optical properties, and magnetic behavior,[9–12] particularly for nylon-6/clay hybrids.[13–15] The clay of a polymer/clay hybrid can be more thoroughly dispersed on a nanometer scale via the insertion of the polymer chains into the silicate interlayers of the clay if the clay is pretreated with an appropriate surfactant.[16] As is well known, polymer chains can be intercalated into the layered silicates of clay either by the insertion of an appropriate monomer and subsequent polymerization or by the direct insertion of polymer chains from the solution or melt.[17] However, the effect of clay (similar to the effect of a nucleating

*Correspondence to:* F.-C. Chang (E-mail: changfc@cc.nctu.edu.tw)

Journal of Polymer Science: Part B: Polymer Physics, Vol. 39, 2097–2107 (2001)

agent) on the crystallization kinetics of sPS has received less attention.

Previous studies have investigated the structure and thermal and mechanical properties of poly(ϵ-caprolactone)/clay and poly(ethylene oxide)/clay hybrids with polymer intercalation from the solution into the montmorillonite.[18,19] The crystallization rate of the metallocene polyethylene (mPE)/clay nanocomposites is slower than that of pure mPE;[20] the organically modified clay mineral (clay/surfactant) can accelerate the crystallization rate of mPE/clay.[20]

Fourier transform infrared (FTIR) spectroscopic techniques have been extensively applied to assess polymer crystallinity and chain conformation. As a highly effective means of structurally characterizing polymers, FTIR complements other techniques in providing detailed information about chain conformation changes and the crystallinity of crystalline polymers that are nondestructive and fast.[21]

We prepared sPS/clay nanocomposites with polymer intercalation from both solution and melt. Both transmission electron microscopy (TEM) and X-ray diffraction were used to characterize clay dispersibility in the sPS matrix. Solid-state FTIR was used to characterize the changes in the crystalline form and crystallinity in the sPS containing clay. Isothermal differential scanning calorimetry (DSC) analyses were also conducted to examine the effect of the clay content and clay/surfactant cation-exchange ratio on the crystallization behavior of the sPS/clay nanocomposites.

## EXPERIMENTAL

### Materials

sPS was kindly supplied by the Industrial Technology and Research Institute of Taiwan; it was synthesized with a homogeneous catalyst consisting of $CpTiCl_3$ and methylalumoxane in toluene,[5] with a number-average molecular weight of 100,000. The chemical structure of sPS with [rr] = 99% was identified with a solution $^{13}C$ NMR spectrum. Kunipia F montmorillonite (clay) was supplied by Kunimine Co. (Japan). This clay mineral possessed exchangeable sodium ions with an exchange capacity of about 119 mequiv per 100 g. Cetyl pyridium chloride (CPC), a cationic surfactant, was purchased from Sigma with a purity greater than 99%.

### Preparation of the Organophilic Clay Mineral

CPC (0.8, 0.4, 0.2, or 0.1 g), 1 g of sodium montmorillonite, and 50 mL of distilled water were placed in a 100-mL beaker; this gave equivalent clay/CPC ratios of 1/2, 1/1, 1/0.5, or 1/0.25. The mixture was stirred vigorously for 8 h and then was filtered, washed, freeze-dried, and kept in a vacuum oven at room temperature for 24 h. This organically modified clay, denoted clay/CPC in the following text, was hydrophobic.

### Preparation of the sPS/Clay Hybrids

Well-dried and predetermined quantities of sPS powder and clay or clay/CPC were added to dichlorobenzene and then stirred at 140 °C for 24 h. The mixture was dried in a vacuum oven at 140 °C for 24 h, and a film was obtained. Melt blending of the sPS and clay or clay/CPC was carried out on a corotating, 30-mm, twin-screw extruder (L/D = 36; Sino-Alloy Machinery, Inc.). The extruder barrel temperatures were set from 270 to 290 °C, and a rotational speed of 250 rpm was employed. The blended pellets were dried and injection-molded into various 1/8-in. ASTM testing specimens on an Arburg 3-oz injection-molding machine.

### Characterizations

#### *Wide-Angle X-Ray Diffraction*

X-ray diffraction spectra were collected on a X-ray diffraction instrument (M18XHF-SRA., MacScience Co., Japan) with Co K$\alpha$ radiation, and Bragg's Law ($\lambda = 2d \sin \theta$) was used to compute the spacing.

#### *TEM*

TEM micrographs were taken from a microtomed section of sPS/clay hybrids 60–100 nm thick mounted in epoxy with a transmission electron microscope (JEM-2000FX, JOEL Co., Japan) with an acceleration voltage of 100 kV.

#### *DSC Isothermal Crystallization*

A PerkinElmer DSC-7 differential scanning calorimeter was employed for the kinetics of crystallization. The sPS/clay hybrid, with about 5–10 mg in an alumina pan, was heated in a DSC furnace to 320 °C and kept at that temperature for 10 min to ensure total relaxation of the sample and to eliminate the influence of thermal history. The

sample was quickly cooled to the preset crystallization temperature at 240 °C to initiate the isothermal crystallization.

### *Infrared Spectra*

Infrared spectra were obtained at a resolution of 1.0 $cm^{-1}$ with FTIR (Nicolet Avatar 320 FTIR spectrometer, United States) at 30 °C, ranging from 4000 to 400 $cm^{-1}$. The frequency scale was internally calibrated with a He–Ne laser, and 32 scans were single-averaged to reduce the noise. The isothermal experiment was carried out in an environmental chamber with a temperature-programmable controller to an accuracy of ±0.1 °C. The thickness of the sPS sample was controlled at less than 10 $\mu$m to minimize the effect of thickness on crystallization. For melt crystallization, the sPS hybrid was heated at 320 °C for 10 min and then quickly cooled to the preset crystallization temperature at 240 °C. All the sample preparations were under a continuous nitrogen flow to ensure minimal sample oxidation or degradation.

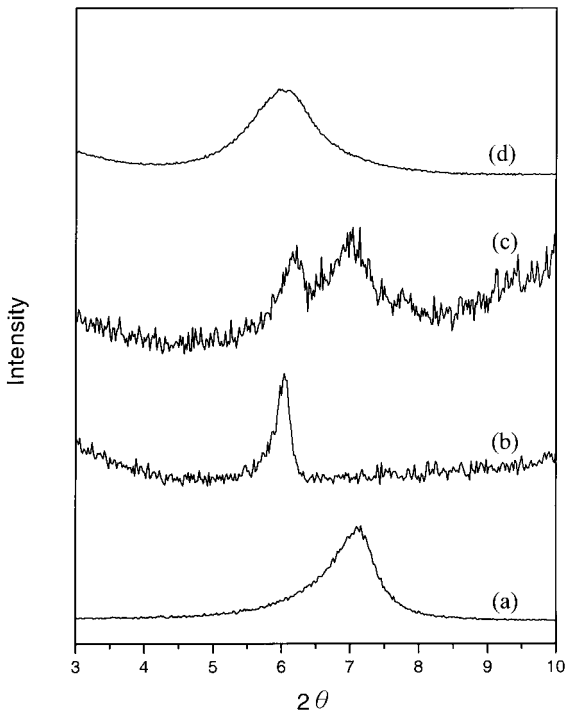


**Figure 1.** X-ray diffraction patterns in a range of $2\theta$ = 3–10° for (a) pure clay, (b) pure $\beta$ form of sPS, (c) 95/5 sPS/clay, and (d) 95/5 sPS/clay–CPC (clay/CPC =1/1).

## RESULTS AND DISCUSSION

### Dispersibility of Clay in the sPS/Clay Hybrids

The clay dispersibility in the sPS matrix was obtained from X-ray diffraction patterns. Figure 1(a–d) presents X-ray diffraction patterns for clay, pure sPS, 95/5 sPS/clay, and 95/5 sPS/clay–CPC (clay/CPC = 1/1) in a range of $2\theta$ = 3–10°. The X-ray diffraction pattern of the pure clay contains basal reflections that are characteristic of the unintercalated repeat distance of $d$ = 1.2 nm ($2\theta$ = 7.1°), as shown in Figure 1(a). One sharp peak, $2\theta$ = 6.1°, appears in Figure 1(b); it corresponds to the pure $\beta$-form sPS crystal.[7,8,21–24] Two peaks, $2\theta$ = 6.9 and 6.1°, shown in Figure 1(c) correspond to the pure clay and $\beta$-form sPS crystal, respectively. Only one broad peak, $2\theta$ = 6.1°, is found in Figure 1(d); it belongs to the $\beta$-form crystal of the sPS, whereas the characteristic peak from the clay disappears totally. With sPS chain intercalation, the layer spacing of the 95/5 sPS/clay–CPC hybrid is less than that of the 1/1 clay/CPC. Therefore, the observed $2\theta$ = 6.1° peak shown in Figure 1(d) should come from the $\beta$-form sPS crystal. Comparing the results from Figure 1(c,d) reveals that the clay appears to be delaminated and dispersed completely within the sPS matrix when the clay is pretreated with the CPC surfactant. Figure 2 shows the X-ray diffraction patterns for various clay/CPC cation-exchange ratios ranging from 1/0 to 1/2. The X-ray diffraction pattern of the pure clay shows the unintercalated repeat distance of $2\theta$ = 7.1°, as shown in Figure 2(a). The peaks ($2\theta$ = 4.1°) appear in Figure 2(d,e) and correspond to 1/1 and 1/2 clay/CPC, indicating that the clay intercalation with CPC is already saturated at clay/CPC = 1/1. In Figure 2(e), the first (001) and major peak appears at $2\theta$ = 4.1°, and the second peak (002) is expected at a double angle (~8.3°). The layer spacing of the clay increases with an increasing CPC content, as shown in Figure 2(b,c). Notably, the difference in compatibility between clay and clay/CPC with sPS significantly affects the formation of the layered structure on the nanoscale level. The sPS chains can be more easily intercalated into the narrow space of the oriented collections of parallel silicate layers by CPC pretreatment.

Figure 3(a,b) shows TEM micrographs of thin sections of 95/5 sPS/clay–CPC and 95/5 sPS/clay hybrids after melt blending. Figure 3(a) contains a TEM bright field image of the sPS/clay–CPC hybrid, where the dark lines denote the silicate layers. The surfactant CPC accommodates the intercalated clay by the organic cation and ren-

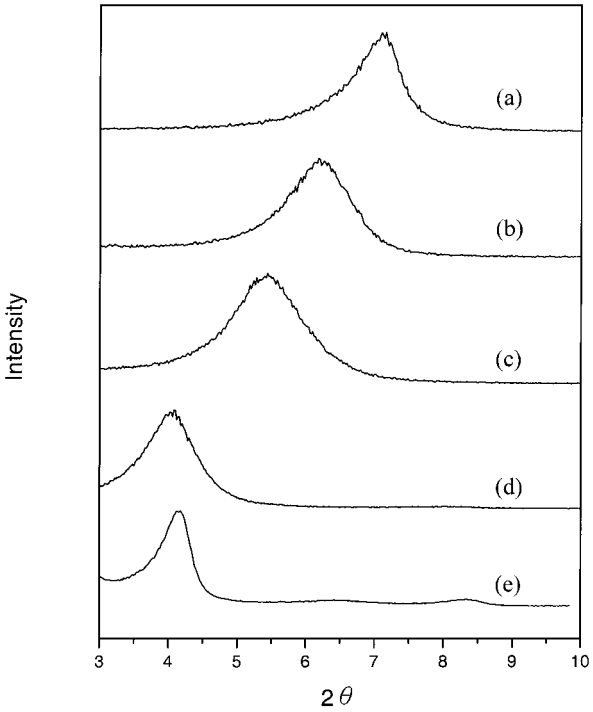


**Figure 2.** X-ray diffraction patterns in a range of $2\theta = 3–10°$ for (a) pure clay, (b) 1/0.25 clay/CPC, (c) 1/0.5 clay/CPC, (d) 1/1 clay/CPC, and (e) 1/2 clay/CPC.

ders the hydrophobic silicate surface organophilic. For sPS/clay–CPC, the stacked silicate layers, about 1–5 nm thick (about one to three parallel silicate layers), are randomly distributed in the sPS matrix. Figure 3(b) reveals that the untreated clay in sPS matrix is not well dispersed, indicating that the layers of clay are unexfoliated. The clay layers from Figure 3(b) are relatively rougher and more agglomerated than those of Figure 3(a). These observations correlate well with the XRD patterns.

### Isothermal Crystallization of sPS/Clay Hybrids

In isothermal DSC operations, the crystallization kinetics of an sPS/clay hybrid is based on Avrami analysis. The following expression is used to measure the extent of crystallization:

$$X(t) = \frac{\int_0^t \frac{dH}{dt}\,dt}{\int_0^\infty \frac{dH}{dt}\,dt} \tag{1}$$

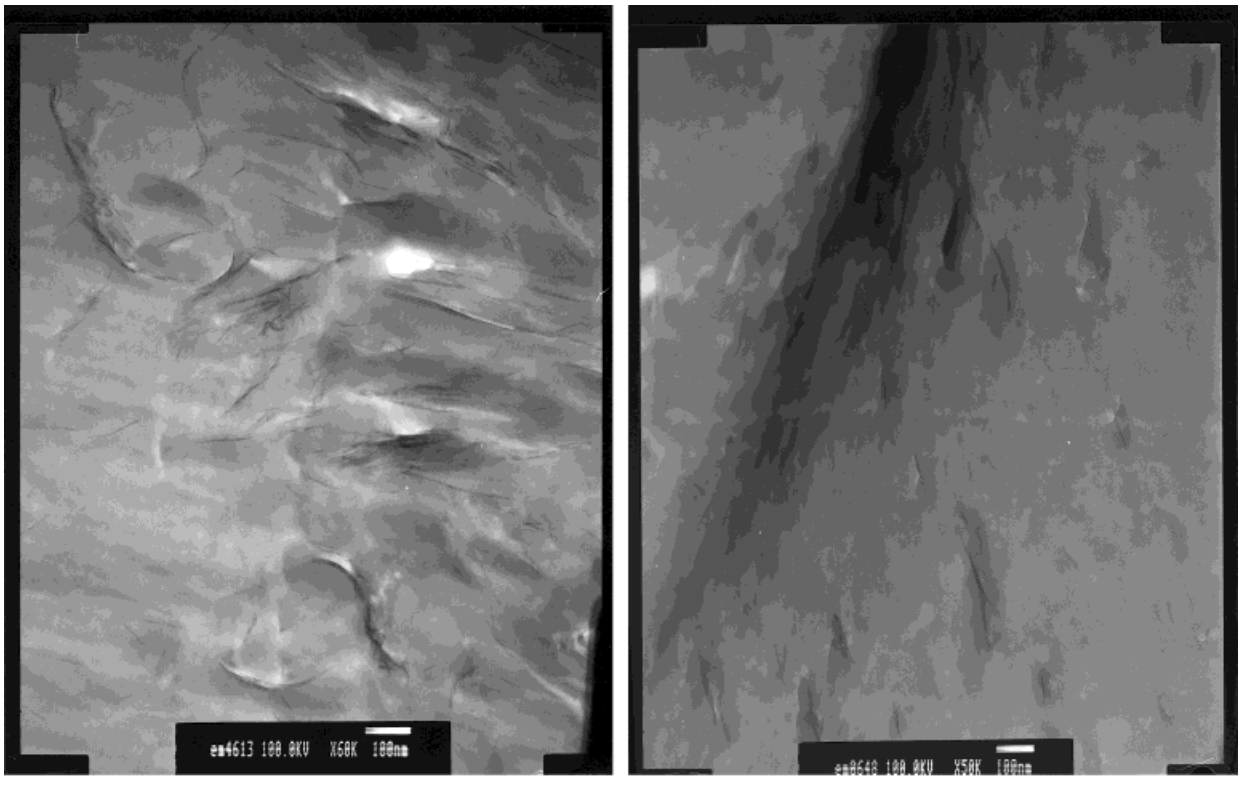


**Figure 3.** TEM micrographs of thin sections of (a) 95/5 sPS/clay–CPC (clay/CPC = 1/1) and (b) 95/5 sPS/clay hybrid obtained from melt blending without thermal treatment.

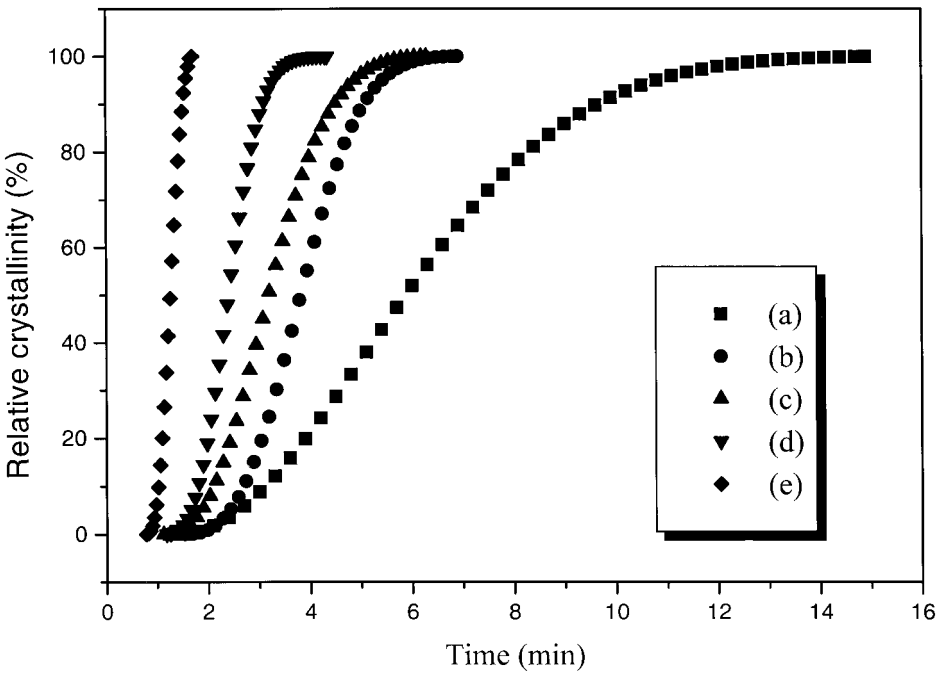


**Figure 4.** Plots of the relative crystallinity versus time at 240 °C for (a) pure sPS, (b) 95/5 sPS/clay–CPC (clay/CPC = 1/1) from solution blending, (c) 95/5 sPS/clay from solution blending, (d) 95/5 sPS/clay–CPC (clay/CPC = 1/1) from melt blending, and (e) 95/5 sPS/clay from melt blending.

where the first integral is the heat generated at time $t$ and the second is the total heat generated up to the end of the crystallization process. By equating the integrals to areas of the isothermal DSC curves, we can shape eq 1 into

$$X(t) = \frac{A_t}{A_\infty} \tag{2}$$

where $A_t$ is the area under the DSC curves from $t = 0$ to $t = t$ and $A_\infty$ is the total area under the crystallization curve. On the basis of this equation, the weight fraction of the crystalline material [$X(t)$] at a specific time can be calculated. Because the crystalline polymer can transform from an amorphous phase to a crystalline phase, $X(t)$ is called the reduced crystallinity. Figures 4–6 plot $X(t)$ versus time for each hybrid at the crystallization temperature (240 °C). The aforementioned results suggest that the clay content, ratio of clay and CPC, and methods for preparing the composite heavily influence the crystallization rate of sPS. By following the Avrami treatment, Figure 4 plots the relative crystallinity as a function of the crystallization times for neat sPS and sPS nanocomposites by different preparation methods. These curves reveal that the crystallization rate of sPS nanocomposites prepared by melt blending [Figs. 4(d,e)] is faster than that of those prepared by solution blending [Figs. 4(b,c)]. Figure 5 plots the relative crystallinity versus crystallization time for sPS/clay–CPC hybrids with different ratios of clay to CPC. A higher clay/CPC ratio [Fig. 5(f)] results in a slower crystallization rate, implying that the presence of CPC, free or intercalated, tends to retard the sPS crystallization. Better compatibility between CPC and sPS makes better clay/CPC dispersion in the sPS matrix and retards the sPS crystallization by physical hindrance of sPS chains. Figure 6 plots the relative crystallinity versus crystallization time for sPS/clay hybrids at different clay contents, indicating that the sPS crystallization rate significantly increases, even with a slight clay content. The pure clay can act as an efficient nucleating agent to facilitate sPS crystallization.

### Effect of Clay on the Overall Kinetic Rate Coefficient ($k$) and Avrami exponent ($n$) Values

The kinetic analysis is performed with the following Avrami equation:

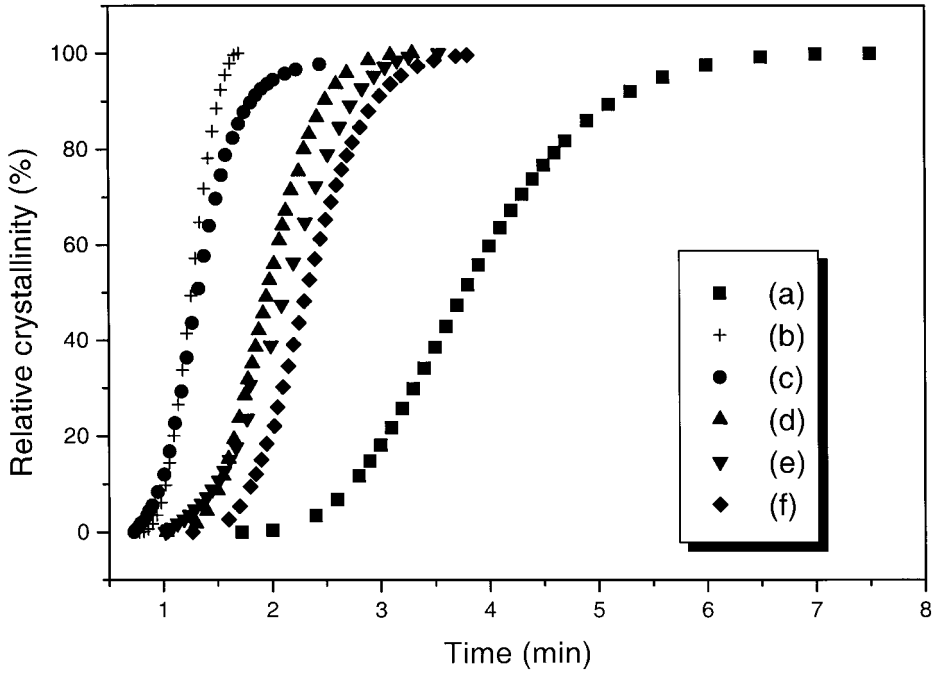


**Figure 5.** Plots of the relative crystallinity versus time for pure sPS and 95/5 sPS/clay–CPC hybrids at 240 °C for various clay/CPC ratios from melt blending: (a) pure sPS, (b) 1/0 clay/CPC, (c) 1/0.25 clay/CPC, (d) 1/0.5 clay/CPC, (e) 1/1 clay/CPC, and (f) 1/2 clay/CPC.

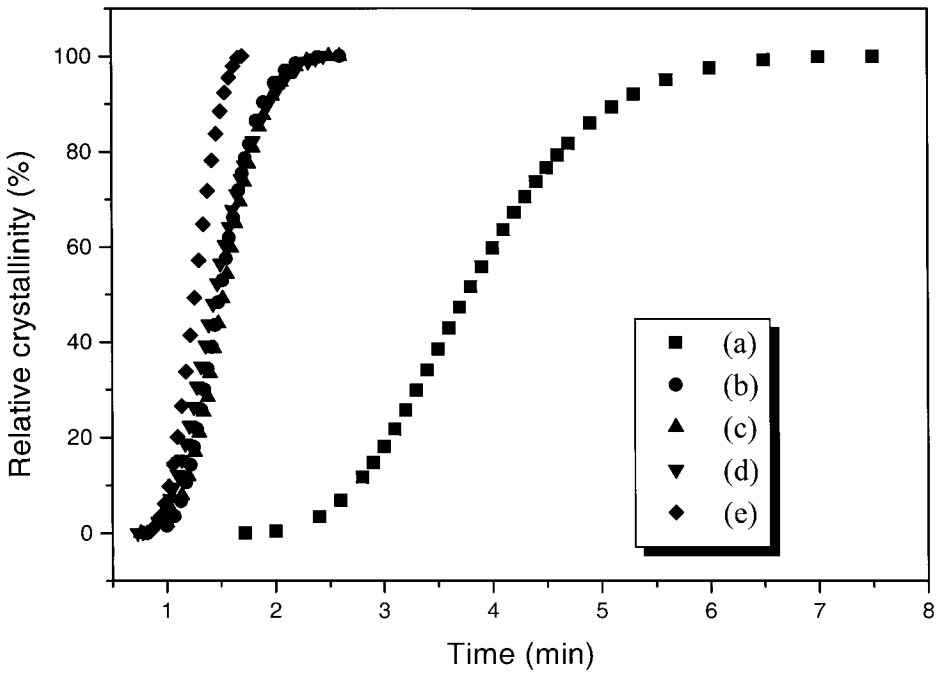


**Figure 6.** Plots of the relative crystallinity versus time for sPS/clay hybrids at 240 °C for various pure clay contents (wt %) from melt blending: (a) pure sPS, (b) 99.5/0.5 sPS/clay, (c) 99/1 sPS/clay, (d) 97.5/2.5 sPS/clay, and (e) 95/5 sPS/clay.

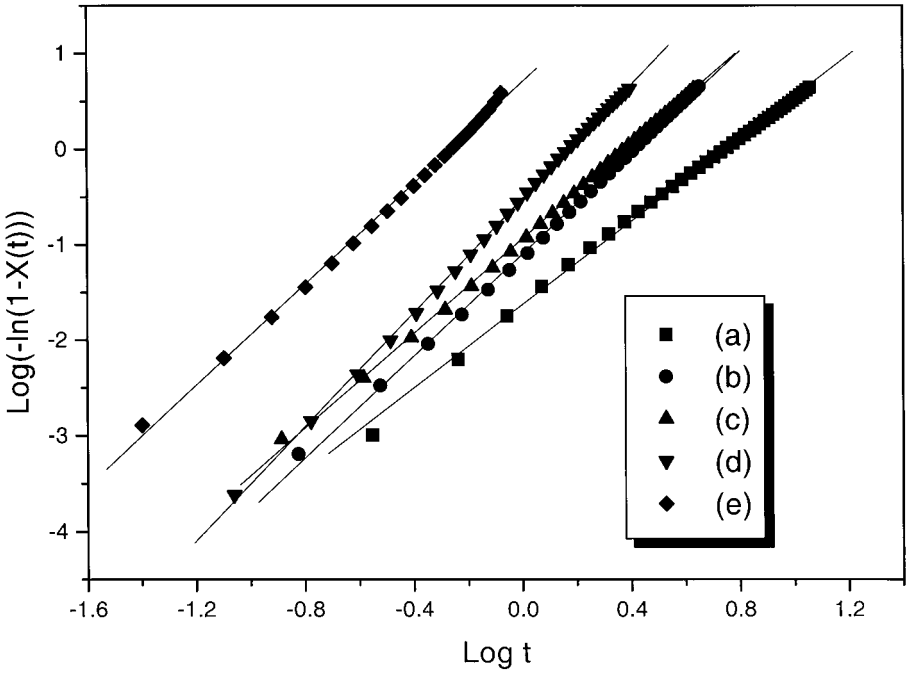


**Figure 7.** Fitting results of crystallization curves of sPS/clay–CPC hybrids by the Avrami model for (a) pure sPS, (b) 95/5 sPS/clay–CPC (clay/CPC = 1/1) from solution blending, (c) 95/5 sPS/clay from solution blending, (d) 95/5 sPS/clay–CPC (clay/CPC = 1/1) from melt blending, and (e) 95/5 sPS/clay from melt blending.

$$X(t) = 1 - \exp(-kt^n) \quad (3)$$

$n$ is a constant that depends on both the nucleation and growth of the crystals and is normally an integer between 1 and 4 for different crystallization mechanisms. By taking logarithms, we can express eq 3 in the following form:

$$\log\{-\ln[1 - X(t)]\} = n \log t + \log k \quad (4)$$

Plotting the first term versus log $t$, we can obtain $k$ and $n$ from the slope and intercept, respectively, at log $t = 0$. Figures 7–9 plot eq 4 for sPS/clay and sPS/clay–CPC hybrids, in which all curves are fitted well by the Avrami equation and result in linear relationships. Table I lists the fitted crystallization kinetic parameters from the slope and intercept of the Avrami plot, $k$, $n$, and the half-life of crystallization ($t_{1/2}$), indicating that pure sPS has the slowest crystallization rate. The crystallization rate not only heavily depends on clay content but also increases with an increasing clay content. For example, when 5% pure clay is added to sPS, the crystallization rate of pristine sPS is increased about 210 times. However, the presence of CPC in the clay tends to retard the rate of crystallization in the sPS/clay hybrid. In these sPS/clay–CPC hybrids, the $k$ value is decreased about 3 times when the ratio of clay to CPC is decreased from 1/0.25 to 1/2. Interestingly, the sPS/clay–CPC hybrid possesses a higher clay dispersion than the sPS/clay hybrid but results in a slower crystallization rate. The CPC molecules may interfere with the nucleation mechanism by physical hindrance within the sPS matrix. The Avrami stretched exponents ($n$) significantly fluctuate with various clay contents (Table I). These silicate layers of the clay (or clay/CPC) may be randomly but not evenly distributed in the sPS matrix, so the obtained $n$ values do not follow any trends. This result is based on isolated bundles growing in a fixed direction in a two-dimensional spacing between silicate layers and should hold for the initial stages of spherulitic crystallization where bundles first form.[25] $t_{1/2}$ decreases exponentially with an increasing clay content or a decreasing clay/CPC ratio, indicating that the crystallization rate is faster when unintercalated clay is added. A higher clay content increases the sPS crystallization rate by shifting the nucleation mechanism from homogeneous nucleation at the homopolymer to heterogeneous nucleation.

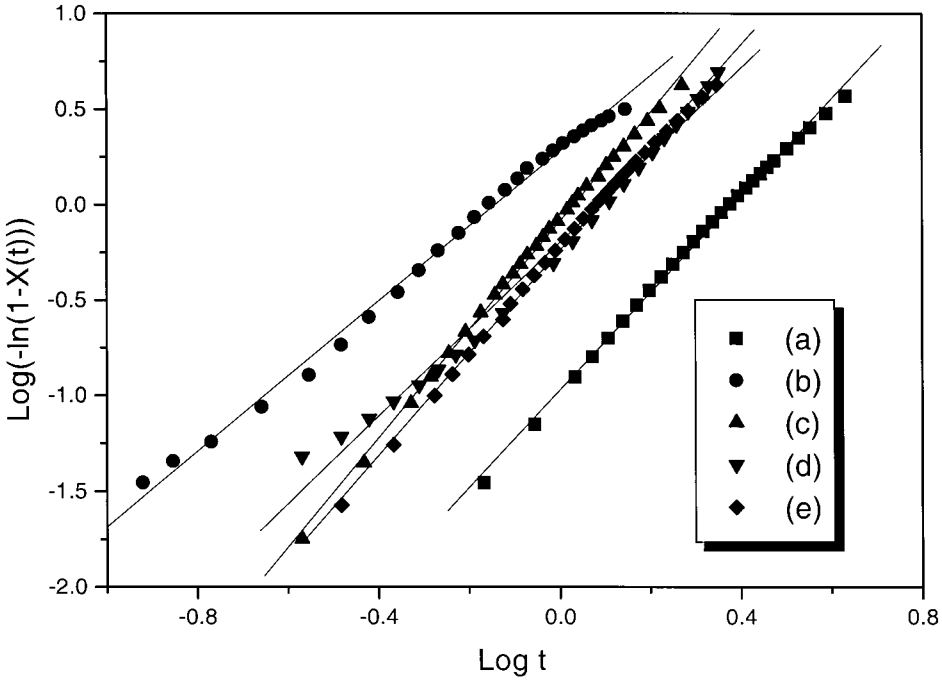


**Figure 8.** Fitting results of crystallization curves of 95/5 sPS/clay–CPC hybrids by the Avrami model for various clay/CPC ratios from melt blending: (a) pure sPS, (b) 1/0.25 clay/CPC, (c) 1/0.5 clay/CPC, (d) 1/1 clay/CPC, and (e) 1/2 clay/CPC.

### Effects of Clay on the Crystal Form of sPS

Figure 10 presents the FTIR spectra of sPS and sPS/clay and sPS/clay–CPC hybrids prepared by melt and solution blending. For understanding more clearly the changes caused by the addition of clay or clay/CPC surfactant, the infrared spec-

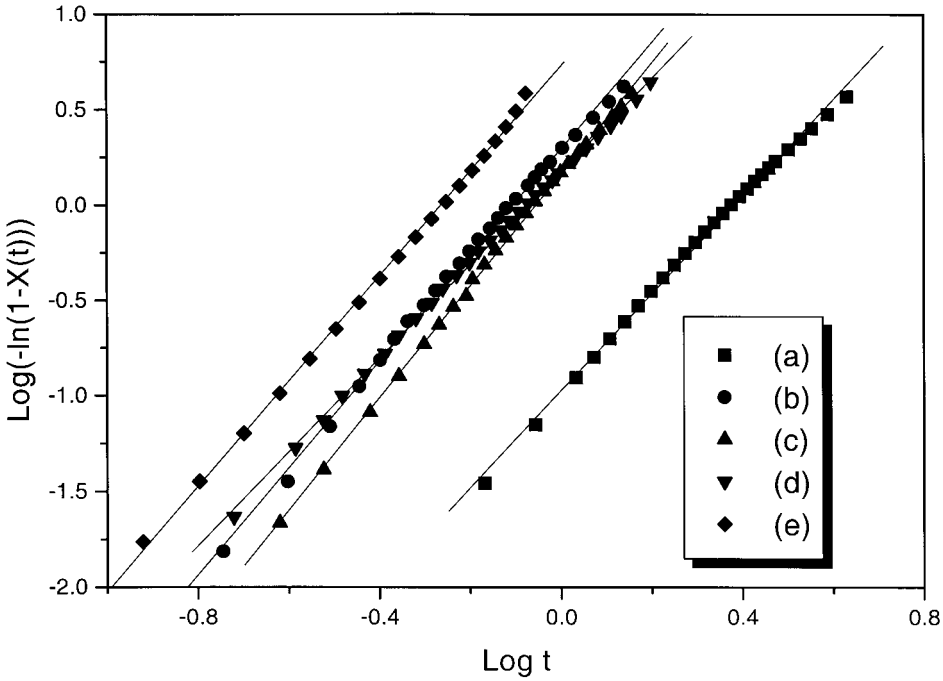


**Figure 9.** Fitting results of crystallization curves of sPS/clay hybrids by the Avrami model for various clay contents (wt %) from melt blending: (a) pure sPS, (b) 99.5/0.5 sPS/clay, (c) 99/1 sPS/clay, (d) 97.5/2.5 sPS/clay, and (e) 95/5 sPS/clay.

**Table I.** Kinetic Parameters for sPS/Clay and sPS/Clay–CPC Hybrids in the Avrami Model

| Composition (%) of sPS/Clay | Clay/CPC Cation-Exchange Ratio | Process | $n$ | $k$ | $t_{1/2}$ (min) |
|---|---|---|---|---|---|
| 100/0 | 0/0 | As received | 2.17 | $2.3 \times 10^{-2}$ | 4.65 |
| 95/5 | 1/1 | Solution | 2.66 | $7.8 \times 10^{-2}$ | 2.28 |
| 95/5 | 1/0 | Solution | 2.47 | 0.12 | 2.07 |
| 95/5 | 1/1 | Melt | 2.28 | 0.63 | 1.10 |
| 95/5 | 1/0 | Melt | 2.64 | 4.90 | 0.48 |
| 100/0 | 0/0 | Melt | 2.54 | 0.11 | 2.04 |
| 95/5 | 1/0.25 | Melt | 1.96 | 1.86 | 0.65 |
| 95/5 | 1/0.5 | Melt | 2.83 | 0.81 | 0.93 |
| 95/5 | 1/1 | Melt | 2.28 | 0.63 | 1.10 |
| 95/5 | 1/2 | Melt | 2.68 | 0.58 | 1.05 |
| 100 | 0/0 | Melt | 2.54 | 0.11 | 2.04 |
| 99.5/0.5 | 1/0 | Melt | 2.78 | 1.95 | 0.68 |
| 99.0/1.0 | 1/0 | Melt | 2.92 | 1.41 | 0.77 |
| 97.5/2.5 | 1/0 | Melt | 2.44 | 1.48 | 0.72 |
| 95.0/5.0 | 1/0 | Melt | 2.64 | 4.90 | 0.48 |

trum, ranging from 940 to 820 $cm^{-1}$, is highly sensitive to chain packing for the sPS polymorph.[24,26–28] The characteristic infrared bands at 905 and 841 $cm^{-1}$ originate from the amorphous phase of sPS.[21] As is well known, the thermodynamically favored $\beta$ form of sPS is formed through melt crystallization at high temperatures.[23] The newborn bands appearing at 911 and 858 $cm^{-1}$ correspond to the $\beta$ crystal when the sPS is melt-crystallized at 240 °C for 10 min and then quenched with liquid nitrogen. The characteristic peaks for the $\alpha$ crystal are absent, as shown in Figure 10(a). Figure 10 also reveals that peak intensities of the $\beta$ crystal (911 and 858 $cm^{-1}$) for sPS/clay and sPS/clay–CPC hybrids prepared by melt blending [Fig. 10(d,e)] are greater than those of the corresponding hybrids prepared by solution blending [Fig. 10(b,c)], implying that the crystallinity of the hybrids prepared by melt blending is higher than that of the corresponding hybrids prepared by solution blending.

Figure 11 shows the DSC thermograms obtained with a heating rate of 10 °C/min from 240 to 310 °C after melt crystallization at 240 °C for 10 min. This special heating scan program attempts to avoid recrystallization at a lower scanning temperature, and the actual melting point of sPS can be obtained from the DSC scan. The melt-crystallized sPS at 240 °C contains one major melting peak at about 271 °C and one minor

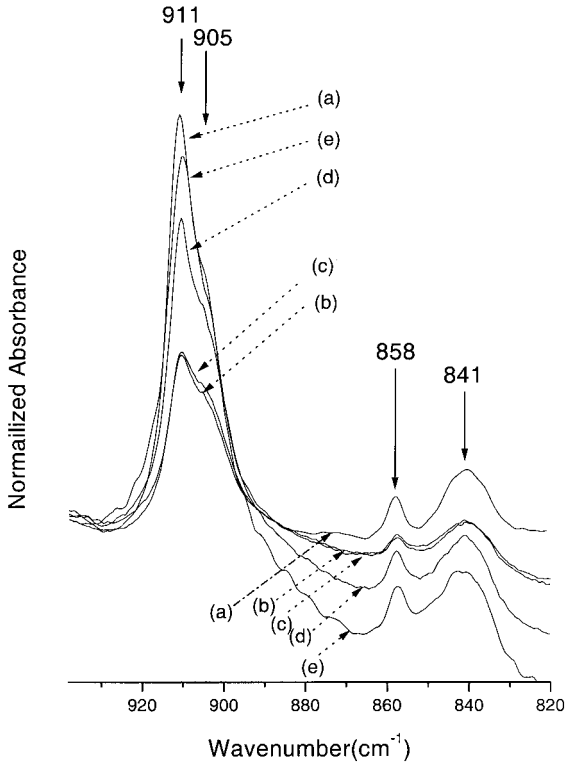


**Figure 10.** FTIR spectra of isothermal melt crystallization at 240 °C for (a) pure sPS, (b) 95/5 sPS/clay from solution blending, (c) 95/5 sPS/clay–CPC (clay/CPC = 1/1) from solution blending, (d) 95/5 sPS/clay from melt blending, and (e) 95/5 sPS/clay–CPC (clay/CPC = 1/1) from melt blending.

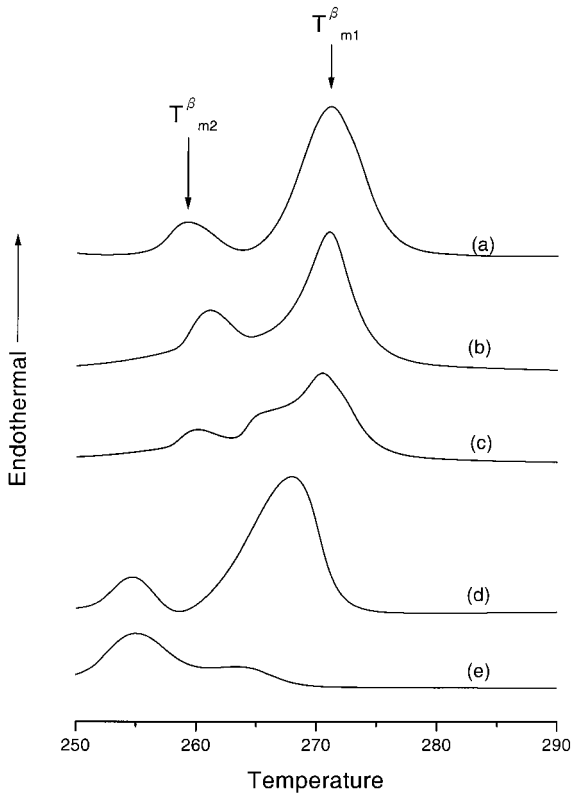


**Figure 11.** DSC thermograms with a scan rate of 10 °C/min for isothermal melt crystallization at 240 °C for (a) pure sPS, (b) 95/5 sPS/clay from solution blending, (c) 95/5 sPS/clay–CPC (clay/CPC = 1/1) from solution blending, (d) 95/5 sPS/clay from melt blending, and (e) 95/5 sPS/clay–CPC (clay/CPC = 1/1) from melt blending.

melting peak at about 259 °C. The major ($T_{m1}^{\beta}$) and minor ($T_{m2}^{\beta}$) melting peaks correspond to the melting of the originally packed thick and thin $\beta$-crystal lamellae, respectively. A portion of the $\beta$ crystal reorganizes into thick lamellae during further crystallization, and the remnant of the crystallized sPS reorganizes as thin lamellae.[21,24] Comparing $T_{m1}^{\beta}$ and $T_{m2}^{\beta}$ reveals that the perfection of the crystallinity of pure sPS in the thick lamellae is higher than that in the thin lamellae. However, for the sPS/clay–CPC hybrid prepared by solution blending, part of the thick $\beta$-crystal phase peak (~271 °C) shifts to about 265 °C. It is proposed that the highly dispersive clay intercalated by sPS chains tends to increase the number of initial nuclei and forms different sizes of $\beta$-crystal lamellae in melt crystallization at 240 °C. Because the clay (or clay/CPC) can act as an efficient nucleating agent to facilitate sPS crystallization, these initial nuclei refer to the primary nucleation. In melt blending, the peaks of $T_{m1}^{\beta}$ and $T_{m2}^{\beta}$ shift to a lower temperature than that in solution blending, as shown in Figure 11(b–e). It has been clearly demonstrated that the presence of clay (or clay/CPC) and the processing method employed significantly affect the nucleus size associated with the morphology of sPS. Figure 11(e) reveals that the thick $\beta$-crystal lamellae have nearly disappeared, and the thinner $\beta$-crystal lamellae dominate when clay/CPC is added to the sPS matrix with better clay dispersity.

## CONCLUSIONS

We have investigated the dispersibility of clay in sPS nanocomposites with wide-angle X-ray diffraction and TEM. Experimental results indicate that sPS chains can intercalate more efficiently into silicate layers when clay is pretreated with CPC as a surfactant. The sPS crystallization rate of sPS/clay hybrids increases with an increasing clay content. The clay functions as a nucleating agent to increase the crystallization rate of the sPS matrix. The crystallization rate of the sPS containing neat clay is faster than the rate for sPS with clay/CPC. The results of this study demonstrate that the better dispersibility of the clay in the sPS matrix increases the interaction between sPS and clay and changes the crystal size of $\beta$-crystal lamellae for sPS.

The authors thank the National Science Council of the Republic of Chain for financially supporting this research under Contract No. NSC-88-2116-E-009-006.

## REFERENCES AND NOTES

1. Ishihara, N.; Semiya, T.; Kuramoto, M.; Uoi, M. Macromolecules 1986, 19, 2464.
2. Ishihara, N.; Kuramoto, M.; Uoi, M. Macromolecules 1986, 21, 3356.
3. Zambelli, A.; Longo, P.; Pellecchia, C.; Grassi, A. Macromolecules 1987, 20, 2035.
4. Kellar, E. J. C.; Galiotis, C.; Andrews, E. H. Macromolecules 1996, 29, 3515.
5. Pellecchia, C.; Longo, P.; Grassi, A.; Ammendola, P.; Zambelli, A. Makromol Chem Rapid Commun 1987, 8, 277.
6. Musto, P.; Tavone, S.; Guerra, G.; De, R. C. J Polym Sci Part B: Polym Phys 1997, 35, 1055.
7. Woo, E. M.; Wu, F. S. Macromol Chem Phys 1998, 199, 2041.

8. Woo, E. M.; Wu, F. S. J Polym Sci Part B: Polym Phys 1998, 36, 2725.
9. Waddell, W. H.; O'Haver, J. H.; Evans, L. R.; Harwell, J. H. J Appl Polym Sci 1995, 55, 1627.
10. Godovski, D. Y.; Sukharev, V. Y.; Volkov, A. V. Phys Chem Solids 1993, 54, 1613.
11. Wang, Y.; Herron, N. J Phys Chem 1991, 95, 525.
12. Yang, W. Opt Commun 1987, 61, 233.
13. Kojima, Y.; Usuki, A.; Kawasumi, M.; Okada, A.; Kurauchi, T.; Kamigaito, O. J Appl Polym Sci 1993, 49, 1259.
14. Usuki, A.; Kojima, Y.; Kawasumi, M.; Okada, A.; Fukushima, Y.; Kurauchi, T.; Kamigaito, O. Mater Res 1993, 8, 1179.
15. Kojima, Y.; Usuki, A.; Kawasumi, M.; Okada, A.; Fukushima, Y.; Kurauchi, T.; Kamigaito, O. Mater Res 1993, 8, 1185.
16. Tseng, C. R.; Wu, J. Y.; Lee, H. Y.; Chang, F. C. Polymer, to appear, 2001.
17. Jeffrey, W. G. Appl Clay Sci 1999, 15, 31.
18. Jimenez, G.; Ogata, N.; Kawai, H.; Ogihara, T. J Appl Polym Sci 1996, 64, 2211.
19. Ogata, N.; Kawakage, S.; Ogihara, T. Polymer 1997, 38, 5115.
20. Huang, S. B.; Huang, W. J.; Chang, F. C.; Chu, P. J. To be submitted for publication, 2001.
21. Wu, H. D.; Tseng, C. R.; Chang, F. C. Macromolecules 2001, 34, 2992.
22. De, R. C.; Rapaccuolo, M.; Guerra, G.; Petraccone, V.; Corradini, P. Polymer 1992, 33, 1423.
23. De, R. C.; Corradini, P. Macromolecules 1993, 26, 5711.
24. Wu, H. D.; Wu, I. D.; Chang, F. C. Macromolecules 2000, 33, 8915.
25. Kit, K. M.; Schultz, J. M. J Polym Sci Part B: Polym Phys 1998, 36, 873.
26. Pellecchia, C.; Longo, P.; Grassi, A.; Ammendola, P.; Zambelli, A. Makromol Chem Rapid Commun 1987, 8, 277.
27. Musto, P.; Tavone, S.; Guerra, G.; De Rosa, C. J Polym Sci Part B: Polym Phys 1997, 35, 1055.
28. Vittoria, V.; Ruvolo Filho, A.; De Candia, F. J Macromol Sci Phys 1990, 29, 411.